Electrical Power and Energy Systems 88 (2017) 108–118

Contents lists available at ScienceDirect

Electrical Power and Energy Systems

journal homepage: www.elsevier.com/locate/ijepes

# Effect of placement of droop based generators in distribution network on small signal stability margin and network loss

D.K. Dheer [a], S. Doolla [a,*], S. Bandyopadhyay [a], Josep M. Guerrero [a,b]

[a] Department of Energy Science and Engineering, Indian Institute of Technology Bombay, Powai, Mumbai 400076, India
[b] Department of Energy Technology, Power Electronic Systems, Aalborg University, 9220 Aalborg, Denmark

ARTICLE INFO

*Article history:*
Received 27 April 2016
Received in revised form 3 November 2016
Accepted 22 December 2016

*Keywords:*
Islanded microgrid
Droop control
Small signal stability margin

ABSTRACT

For a utility-connected system, issues related to small signal stability with Distributed Generators (DGs) are insignificant due to the presence of a very strong grid. Optimally placed sources in utility connected microgrid system may not be optimal/stable in islanded condition. Among others issues, small signal stability margin is on the fore. The present research studied the effect of location of droop-controlled DGs on small signal stability margin and network loss on a modified IEEE 13 bus system, an IEEE 33-bus distribution system and a practical 22-bus radial distribution network. A complete dynamic model of an islanded microgrid was developed. From stability analysis, the study reports that both location of DGs and choice of droop coefficient have a significant effect on small signal stability, transient response of the system and network losses. The trade-off associated with the network loss and stability margin is further investigated by identifying the Pareto fronts for modified IEEE 13 bus, IEEE 33 and practical 22-bus radial distribution network with application of Reference point based Non-dominated Sorting Genetic Algorithm (R-NSGA). Results were validated by time domain simulations using MATLAB.



## 1. Introduction

Growing environmental concerns competitive energy policies has led to the decentralization of power generation. Installations of distributed generators (DGs such as photovoltaic, wind, etc.) are expected to increase worldwide in the next decade [1]. Due to their location being close to consumers, DGs provide better power in terms of quality and reliability [2]. Controllable DGs along with controllable loads present themselves to the upstream network as microgrid. Microgrids when operating in grid-connected mode provide/draw power based on supply/demand within. In islanded mode (when not connected to the main grid), microgrids operate as an independent power system [2].

Optimal location of distributed generators (DGs) in a utility-connected system is well described in literature. The optimality in placement of a DG is decided by the owner based on the availability of primary resource, site, and climatic conditions. Thus, choosing an inappropriate location may result in losses and fall in power quality. Literature has widely addressed optimal placement of DGs in a network based on objective functions of energy/power loss minimization, cost minimization, voltage deviation minimization, profit maximization, loadability maximization, etc. [3]. Different approaches, methods, and optimization techniques for DG siting and sizing are presented in [3–9].

DG siting and sizing is a multi-objective optimization problem classifiable into two groups. The first group focuses on economics of the system [9–17]. With respect to islanded microgrids, minimization of total annual energy losses and cost of energy for distributed generation is an area of much interest to investors [10]. One study [9] presented a multi-objective optimization problem of minimization of photovoltaic, wind generator and energy storage investment cost, expectation of energy not supplied, and line loss. Economic and environmental restrictions for a microgrid are outlined in [11]. Operation cost (local generation cost and grid energy cost) minimization is presented in [12]. An optimization problem considering operation cost and emission minimization is presented in [13]. Economic dispatch problem in a hybrid, droop-based microgrid is presented in [14].

The second group focuses on the optimal design of a microgrid based on technical parameters such as network losses, maximum loadability, voltage profile, reactive power, power quality, and droop setting. The assessment of maximum loadability for a droop-based islanded microgrid is presented in [18–20] considering reactive power requirements and various load types. A combined study on economic as well as on technical aspects is presented in [21]. A decision-making program for load procurement in

* Corresponding author.
*E-mail address:* suryad@iitb.ac.in (S. Doolla).

http://dx.doi.org/10.1016/j.ijepes.2016.12.014
0142-0615/

a distribution network is presented in [22] based on uncertainty parameters like electricity demand, local power investors, and electricity price. To improve the power quality of network, placement and control of unified power quality conditioner in renewable based sources has been introduced and its advantages and disadvantages are discussed in [23]. Optimal setting of droop to minimize the cost of wind generator is presented in [24]. One wind-generation study combined economics and stability issues due to uncertainty (volatility) and its effect on small signal stability [25,26]. This study of small signal stability in droop-based islanded microgrids is thus worthy in the context of potential benefits of optimal DG placement to grid managers.

A microgrid may present as much complexities as a conventional power system. When connected to a grid, these optimally placed and sized DGs (inverter-based) operate in current control mode, feeding maximum power to the network. When a grid is not available, these DGs shift to droop control mode for effective power sharing [27].

Two important aspects of an islanded microgrid load sharing and stability are widely addressed in literature. A higher droop in these DGs is desired for better power sharing and transient response [28–30]. Higher droop and stability margin improves the transient response of the system and hence power sharing among the sources [30]. Inappropriate settings of droop value may cause a power controller to operate at low frequency mode and fall into an unstable region [31,32]. Stability of islanded microgrids is a growing operational challenge. Based on the detailed literature survey it is found that: (1) Effect of placement of sources on stability margin in a droop based islanded microgrid and (2) Optimally placed sources based on network loss minimization in a grid connected system suffers stability problem when it gets islanded is not investigated so far. A grid-connected system optimized for DG sizing and siting may be vulnerable to small signal stability when islanded. This problem is more serious in rural areas of developing countries (e.g. India, sub-saharan Africa, etc.) where load shedding is still a common problem. As these islanded microgrids needs to operate without grid for a long time, stability is main concern. The impact of optimal DG placement on enhancement of small signal stability margin and loss minimization is investigated on a modified IEEE 13-bus low voltage distribution system, a standard IEEE 33-bus distribution system and a practical 22-bus radial distribution network of a local utility.

The paper is organized as follows: Section 2 presents a description of the system considered and the mathematical model designed for stability studies. Eigen value analysis and identified Pareto fronts are presented in Section 3. Validation of Eigen value analysis by time domain simulation is presented in Section 4, followed by conclusions of the study in Section 5.

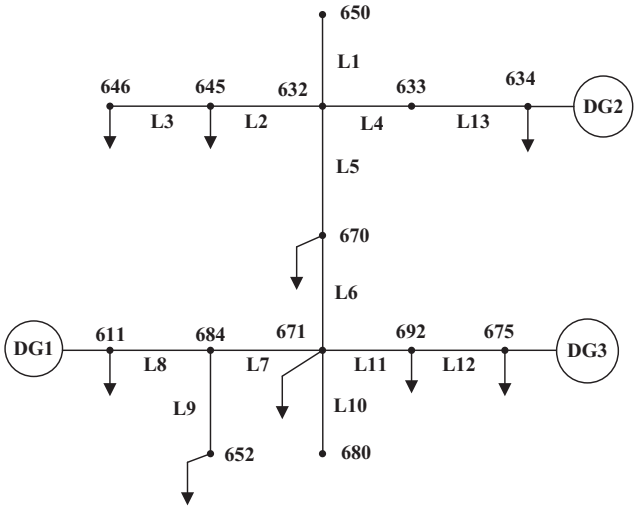


**Fig. 1.** Modified IEEE 13-bus system.

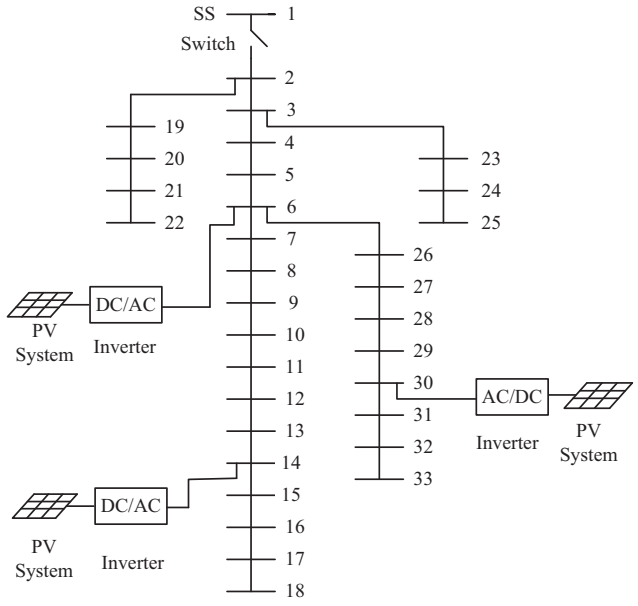


**Fig. 2.** IEEE 33-bus radial distribution system.

## 2. System description and mathematical modeling

Microgrids integrated with renewable energy sources through voltage source inverters (VSIs), together with loads and interconnecting lines, were considered for the present study. A modified IEEE 13-bus system [33] (Fig. 1), IEEE 33-bus radial distribution system [34] (Fig. 2 and a 22-bus practical radial distribution network of Andhra Pradesh Eastern Power Distribution Company Limited (APEPDCL)[35], India (Fig. 3) were considered.

### 2.1. System state space equation

The modeling of VSIs, line, and load in *d-q* axis reference frame for small signal stability is defined in [33,36]. VSI model is divided into four sub-modules: power controller with droop control, voltage controller, current controller and LC-filter with coupling inductor. All the sources are operating in conventional droop (P-f and Q-V) to share the power as per their rating:

$$\omega = \omega_n - m_p P \tag{1}$$

$$V = V_n - n_q Q \tag{2}$$

where $\omega_n, V_n$ are nominal frequency and voltage, P and Q are filtered real and reactive power and $m_p$ and $n_q$ are active and reactive power droop coefficients respectively. Eq. (3) is the overall state space (matrix) equation for the total system under consideration. For the IEEE 33-bus system, the size of matrix $A_{MG}$ with two generators is 152 × 152, which includes 26 states of DGs, 62 states of lines, and 64 states of loads. With three generators, the size of $A_{MG}$ is 165 × 165 (39 states of DGs, 62 states of lines, and 64 states of loads). Similarly, for the 22-bus practical radial distribution network of APEPDCL, the size of $A_{MG}$ with three generators is 121 × 121 (39 states of DGs, 40 states of lines, and 42 states of loads).

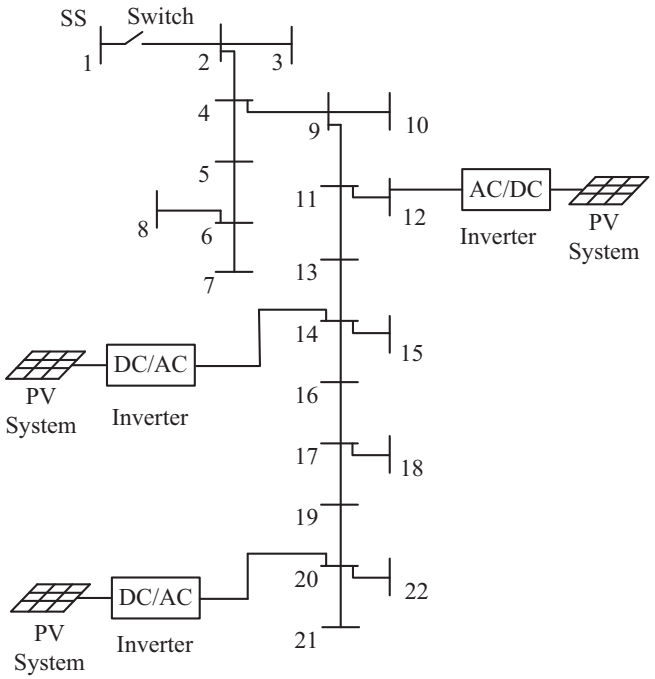


**Fig. 3.** Practical radial distribution (22 bus) network APEPDCL.

$$\begin{bmatrix} \Delta \dot{X}_{DG} \\ \Delta I_{DQ_{Line}} \\ \Delta I_{DQ_{Load}} \end{bmatrix} = A_{MG} \begin{bmatrix} \Delta X_{DG} \\ \Delta I_{DQ_{Line}} \\ \Delta I_{DQ_{Load}} \end{bmatrix} \tag{3}$$

where $[\Delta X_{DG}]$ is combined states of all the inverters based sources, $[\Delta I_{DQ_{Line}}]$ and $[\Delta I_{DQ_{Load}}]$ are combined states of all the lines and loads in the network.

### 2.2. Loss calculation

Consider a line of impedance $(R + jX)\ \Omega$ connected between two nodes through which current $I_i$ is flowing. This current $(I_i)$ can be expressed as:

$$I_i = I_d \pm jI_q \tag{4}$$

Real power loss in the line can be calculated using:

$$P_{loss,i} = I_i^2 \times R_i \tag{5}$$

where $I_i^2 = I_d^2 + I_q^2$. Total real power loss of the network containing $n$ lines is the sum of individual line loss which is

$$P_{loss} = \sum_{i=1}^{n} P_{loss,i} \tag{6}$$

### 2.3. Small signal stability margin

In this study, small signal stability margin is related to droop parameters. Higher droop is desired for better power sharing and transient response. The system is said to be stable if the real part of all eigenvalues are negative.

In this study, droop parameters ($m_p$ and $n_q$) are taken as system variables. The droop constants are designed using (7) and (8). For the present work, initial values of $m_p$ and $n_q$ are taken as $1.0 \times 10^{-6}$ rpm/W and $1.0 \times 10^{-5}$ V/VAR, respectively.

$$m_{p1} \times P_1 = m_{p2} \times P_2 = \cdots = m_{pn} \times P_n \tag{7}$$

$$n_{q1} \times Q_1 = n_{q2} \times Q_2 = \cdots = n_{qn} \times Q_n \tag{8}$$

To perform Eigen value analysis, draw the root locus plot and calculate the losses, we obtain the operating condition/point using time domain simulation or from load flow analysis. Literature on load flow analysis for islanded systems is scarce. In the present study, time domain simulation is performed by using MATLAB/SIMULINK to obtain the operating point. The time domain simulation is also used to validate the Eigen value analysis.

### 2.4. Problem formulation for multiobjective optimization for islanded microgrid

It is widely accepted that simulation based multiobjective problems are difficult to solve which is caused by vast number of simulation runs that are needed in order to find a converged and diverse set of Pareto-optimal solution [37–39]. For such studies a Reference point based Non-dominated Sorting Genetic Algorithm-II (R-NSGA-II) is generally used [37]. In the present study R-NSGA-II is implemented to obtain Pareto front by keeping stability margin and power loss as multiobjectives. Flow chart for R-NSGA-II is shown in Fig. 4.

The multiobjective problem consists of two objectives: real power loss minimization and small signal stability margin maximization.

$$f_1 = \sum_{i=1}^{n} \left(I_{di}^2 + I_{qi}^2\right) R_i \tag{9}$$

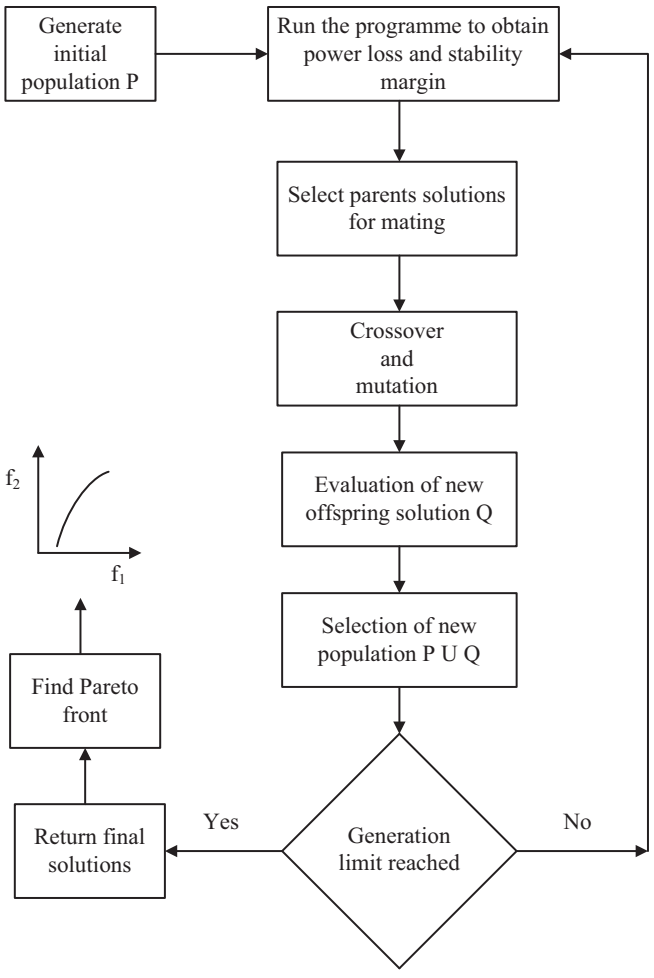


**Fig. 4.** R-NSGA-II flow chart.

where $f_1$ is over all real power loss and n is the total number of lines in the network as given in Eq. (5).

$$f_2 = m_P * p \tag{10}$$

where $f_2$ is small signal stability margin, $m_P$ is the initial value of power-frequency droop and $p$ is multiplying factor. Higher value of $p$ represents higher stability margin subjected to the system stability.

Constraints for the optimization problem are:

$$V_{min} \leqslant V \leqslant V_{max} \tag{11}$$

where $V_{min}$ is 0.9 p.u. and $V_{max}$ is 1.02 p.u.

$$f_{min} \leqslant f \leqslant f_{max} \tag{12}$$

where $f_{min}$ is 48.5 Hz and $f_{max}$ is 50 Hz.

$$R[\lambda_i] < 0 \tag{13}$$

where $\lambda_i$ is the $i$th eigenvalue of the system and $R[\lambda_i]$ is the real part of that eigenvalue.

## 3. Eigen value analysis and Pareto front identification for modified IEEE 13-bus, IEEE 33-bus and practical 22-bus distribution systems

### 3.1. System-1: Modified IEEE 13-bus system with three DGs

To achieve the Pareto front based on small signal stability margin and real power loss as multi-objectives, reference nodes (locations for DGs) are generated and R-NSGA-II is implemented as shown in flow chart given in Fig. 4.

Fig. 5 shows the return final solution after generation limit is reached. From this final solution, Pareto front is obtained which is shown in Fig. 6. Results corresponding to the Pareto front (Fig. 6) is presented in Table 1. Initial value of $m_P$ is taken as $6.0 \times 10^{-5}$.

### 3.2. System-2: IEEE 33-bus system with two DGs

The optimal locations of two generators (in a grid-connected system) based on loss minimization proposed in [40] are at nodes 6 and 30. When islanded, these two generators operate in droop control mode (for size in proportion of 1:0.50) for load sharing. From the droop law, we know that system frequency takes a new steady state value till secondary control acts. System simulation (time domain) is performed with these two generators at various locations (cases) in a standard IEEE 33-bus radial distribution network. From the operating points, state space matrix is obtained

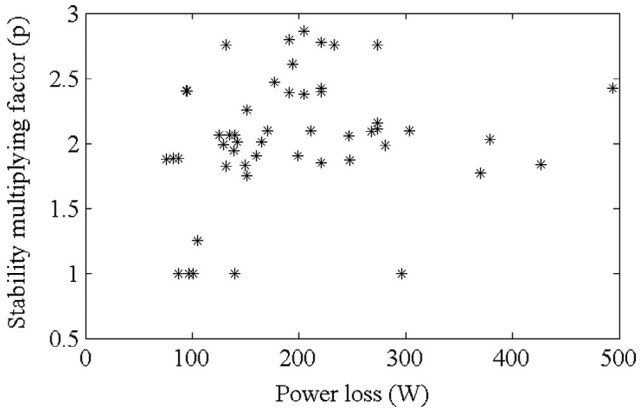


**Fig. 5.** Conversed solutions with R-NSGA-II.

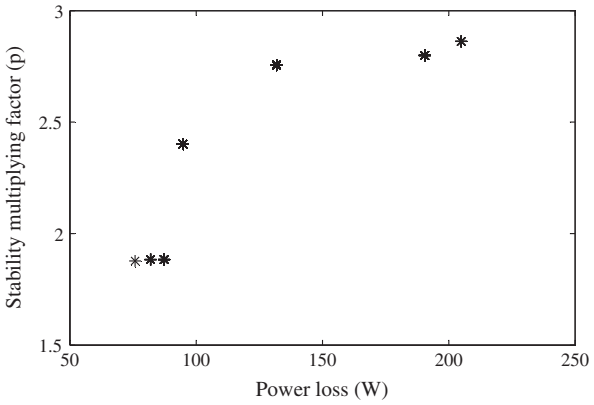


**Fig. 6.** Pareto front for modified IEEE 13-bus system.

using (3). Root locus analysis is performed for these cases by varying the droop constants to identify the stability limit. The values of $m_{p,max}$ and $n_{q,max}$ are noted when the system reaches an unstable region. Losses in the system, minimum voltage value in the total network, $m_{p,max}, n_{q,max}$, and minimum distance between the DGs for all these cases are presented in Table 2. It is clear that the maximum values of $m_{p,max}$ and $n_{q,max}$ are not the best for case 1. This is true since the decision for placement of generators in this location in [40] was made with separate conditions (grid-connected, exporting power, etc.). However, in systems where grid reliability is poor (true in many developing countries), such location may not be optimum. From network loss, stability, and voltage perspectives, case 1, case 6, and case 13 are preferred options, respectively.

#### 3.2.1. Effect of distance between generators on stability margin

While conducting the eigenvalue analysis for the system considered, electrical distance between the generators is measured (Table 2). Fig. 7 shows the plot between $m_{p,max}$ and Z, while Fig. 8 shows the plot between $n_{q,max}$ and Z for the cases tabulated in Table 2. Electrical distance (in terms of impedance) between generators is an important parameter contributing to small signal stability margin. From Figs. 7 and 8, it is observed that higher electrical distance between sources results in better stability margin. Root locus plot and time domain simulation further prove this point. Case 1 (base case), case 6 (highest stability margin), and case 18 (least stability margin) are considered for detailed analysis.

#### 3.2.2. Rootlocus analysis

Fig. 9 shows the root locus plot of the system for case −1, case −6, and case −18. $\lambda_{12}$ indicates the interaction of low-frequency modes between two sources. From the three sets of Eigen traces, it s clear that the system is going into an unstable region after a certain value of $m_P$. In Fig. 9, $\lambda_{12}$ for case −1 starts from $-15.066 \pm j\ 16.60$ and reaches the imaginary axis at $0 \pm j\ 74.40$, while for case −6 and case −18 the starting points for $\lambda_{12}$ are at $-15.346 \pm j\ 1.1835$ and $-12.971 \pm j\ 28.278$ and they reach the imaginary axis at $0 \pm j\ 87.05$ and $0 \pm j\ 58.84$, respectively. From these root locus plots, the effect of impedance between sources on stability margin is observed, and it is clear that, distance between sources influences the stability of the system.

### 3.3. System-3: IEEE 33-bus system with three DGs

Optimal locations of three generators (in grid connected system) based on loss minimization, proposed in [40], are at nodes 6, 14, and 30. When islanded, these three generators operate in droop control mode for load sharing. System simulation (time

**Table 1**
Results for Pareto front obtained for modified IEEE 13-bus system with three sources.

| Node | Node | Node | $P_{loss}$ (W) | Stability multiplying factor (p) | Stability margin $m_{p,max}$ ($10^{-5}$) |
|---|---|---|---|---|---|
| 632 | 692 | 675 | 75.86 | 1.8776 | 11.2656 |
| 645 | 692 | 675 | 81.94 | 1.8836 | 11.3016 |
| 692 | 675 | 634 | 87.33 | 1.8839 | 11.3034 |
| 633 | 684 | 675 | 94.80 | 2.4022 | 14.4252 |
| 670 | 680 | 675 | 131.86 | 2.7559 | 16.5354 |
| 645 | 633 | 675 | 190.52 | 2.7993 | 16.7958 |
| 645 | 633 | 692 | 204.956 | 2.8662 | 17.1972 |

**Table 2**
Various case study results for two DGs placement for IEEE 33-bus radial network.

| Case | DG-1 node | DG-2 node | $P_{loss}$ (kW) | $V_{min}$ (p.u.) | $m_{p,max}$ ($10^{-5}$) | $n_{q,max}$ ($10^{-4}$) | Z (Ω) |
|---|---|---|---|---|---|---|---|
| 1 | 6 | 30 | 65.05 | 0.9469 | 1.24 | 1.34 | 3.5709 |
| 2 | 24 | 30 | 74.27 | 0.9303 | 2.30 | 2.21 | 7.1671 |
| 3 | 18 | 24 | 120.48 | 0.9193 | 4.90 | 5.92 | 16.8053 |
| 4 | 13 | 30 | 264.07 | 0.9206 | 3.43 | 2.84 | 11.1844 |
| 5 | 18 | 25 | 143.45 | 0.9068 | 5.33 | 6.10 | 17.9422 |
| 6 | 18 | 22 | 207.91 | 0.8855 | 5.55 | 6.31 | 19.6787 |
| 7 | 22 | 33 | 185.24 | 0.9003 | 3.39 | 3.84 | 12.4616 |
| 8 | 22 | 25 | 175.09 | 0.8906 | 2.08 | 2.72 | 7.3835 |
| 9 | 25 | 33 | 106.39 | 0.9131 | 3.16 | 3.48 | 10.7276 |
| 10 | 18 | 33 | 386.46 | 0.8833 | 5.39 | 4.58 | 19.2281 |
| 11 | 6 | 14 | 83.96 | 0.9528 | 2.44 | 3.12 | 8.4827 |
| 12 | 6 | 18 | 120.38 | 0.9524 | 3.60 | 5.08 | 0.9524 |
| 13 | 6 | 10 | 72.29 | 0.9532 | 1.53 | 1.97 | 5.1831 |
| 14 | 3 | 5 | 97.04 | 0.9335 | 0.88 | 0.37 | 0.8118 |
| 15 | 6 | 26 | 84.97 | 0.9487 | 0.82 | 0.23 | 0.2278 |
| 16 | 3 | 4 | 103.26 | 0.9273 | 0.80 | 0.27 | 0.4107 |
| 17 | 9 | 10 | 238.42 | 0.8823 | 0.73 | 0.59 | 1.2764 |
| 18 | 32 | 33 | 291.85 | 0.8507 | 0.43 | 0.47 | 0.6304 |
| 19 | 17 | 18 | 525.83 | 0.7425 | 0.65 | 0.50 | 0.9302 |
| 20 | 24 | 25 | 182.31 | 0.8890 | 0.66 | 0.58 | 1.1377 |

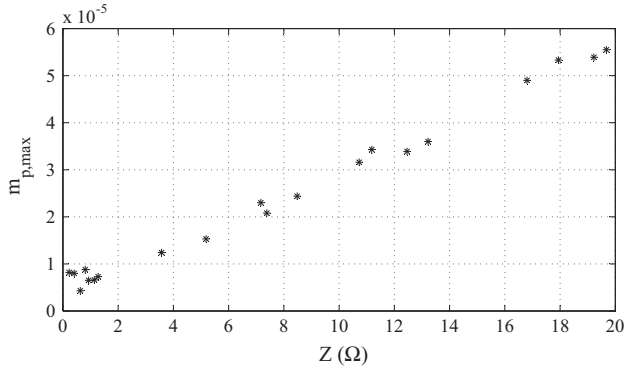


**Fig. 7.** Impedance vs. $m_{p,max}$ plot.

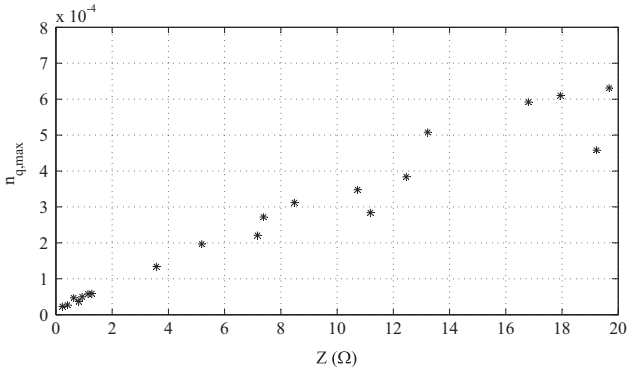


**Fig. 8.** Impedance vs. $n_{q,max}$ plot.

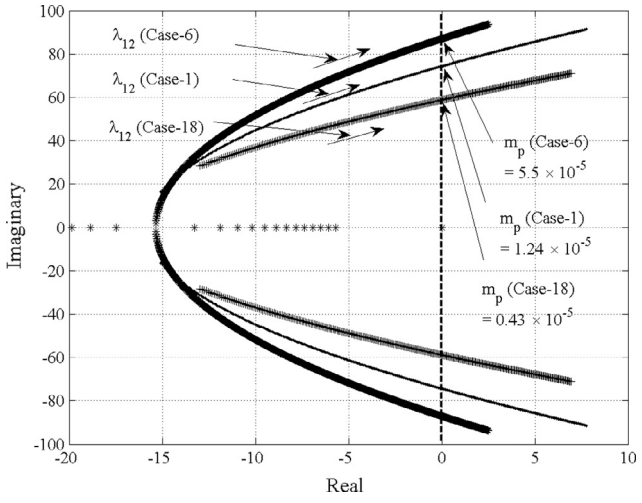


**Fig. 9.** System-2: cases-1, 6, 18: Rootlocus plot with variation in droop gain $m_p$.

domain) is performed with these three generators at various locations (cases) in a standard IEEE 33 bus radial distribution network. From the operating points, state space matrix is obtained using (3). Root locus analysis is performed for these cases by varying droop constants to identify the stability limit. The values of $m_{p,max}$ and $n_{q,max}$ are noted when the system reaches an unstable region. Losses in the system, minimum voltage value in the total network, $m_{p,max}, n_{q,max}$ and minimum distance between the DGs for all these cases are presented in Table 3.

It is clear that the maximum values of $m_{p,max}, n_{q,max}$ are not the highest for case-1. This is true since the decision for this location

**Table 3**
Various case study results for three DGs placement for IEEE 33-bus radial network.

| Case | DG-1 node | DG-2 node | DG-3 node | $P_{loss}$ (kW) | $V_{min}$ (p.u.) | $m_{p,max}$ ($10^{-5}$) | $n_{q,max}$ ($10^{-4}$) | $Z_{min}$ (Ω) |
|---|---|---|---|---|---|---|---|---|
| 1 | 6 | 30 | 14 | 60.03 | 0.9581 | 1.81 | 1.31 | 3.5709 |
| 2 | 25 | 33 | 18 | 67.98 | 0.9635 | 2.91 | 4.12 | 10.7274 |
| 3 | 22 | 33 | 18 | 86.76 | 0.9441 | 2.94 | 4.73 | 12.4616 |
| 4 | 24 | 30 | 8 | 32.36 | 0.9694 | 0.92 | 1.80 | 6.1455 |
| 5 | 24 | 30 | 18 | 44.86 | 0.9751 | 2.38 | 2.62 | 7.1671 |
| 6 | 6 | 30 | 18 | 79.30 | 0.9577 | 1.78 | 1.38 | 3.4992 |
| 7 | 24 | 30 | 6 | 45.94 | 0.9530 | 0.53 | 0.76 | 3.5965 |
| 8 | 24 | 30 | 22 | 52.07 | 0.9364 | 1.35 | 2.05 | 6.2483 |
| 9 | 24 | 6 | 18 | 84.58 | 0.9613 | 1.22 | 1.29 | 3.5965 |
| 10 | 10 | 30 | 15 | 126.06 | 0.9347 | 1.19 | 1.31 | 4.0902 |
| 11 | 10 | 24 | 15 | 153.56 | 0.9360 | 1.18 | 1.30 | 4.0902 |
| 12 | 10 | 22 | 15 | 151.49 | 0.9167 | 1.19 | 1.35 | 4.0902 |
| 13 | 24 | 30 | 20 | 45.87 | 0.9370 | 1.08 | 1.50 | 4.4788 |
| 14 | 24 | 20 | 18 | 95.61 | 0.9321 | 1.80 | 1.84 | 4.4788 |
| 15 | 24 | 30 | 3 | 46.11 | 0.9471 | 0.54 | 0.57 | 1.6905 |
| 16 | 24 | 3 | 18 | 75.06 | 0.9422 | 0.44 | 0.16 | 1.6905 |
| 17 | 24 | 21 | 3 | 135.0 | 0.9235 | 0.43 | 0.53 | 1.6905 |
| 18 | 24 | 22 | 18 | 114.78 | 0.9299 | 2.23 | 2.62 | 6.2483 |
| 19 | 6 | 11 | 18 | 212.26 | 0.9554 | 0.94 | 1.71 | 5.3783 |
| 20 | 2 | 6 | 18 | 65.20 | 0.9617 | 1.07 | 0.97 | 2.456 |
| 21 | 24 | 21 | 2 | 139.08 | 0.9181 | 0.40 | 0.59 | 2.2352 |
| 22 | 2 | 6 | 30 | 36.66 | 0.9528 | 0.61 | 0.79 | 2.456 |
| 23 | 24 | 21 | 6 | 96.28 | 0.9509 | 0.82 | 1.04 | 3.5965 |
| 24 | 8 | 14 | 18 | 362.75 | 0.9062 | 0.62 | 1.46 | 4.7548 |
| 25 | 2 | 4 | 6 | 76.63 | 0.9514 | 0.41 | 0.42 | 0.964 |
| 26 | 24 | 21 | 11 | 91.14 | 0.9409 | 1.63 | 2.01 | 5.0983 |
| 27 | 7 | 26 | 30 | 64.41 | 0.9514 | 0.64 | 0.26 | 0.8209 |
| 28 | 10 | 14 | 18 | 386.80 | 0.8604 | 0.60 | 1.16 | 3.2999 |
| 29 | 3 | 6 | 11 | 41.92 | 0.9627 | 0.72 | 0.77 | 2.3629 |
| 30 | 3 | 6 | 30 | 34.80 | 0.9532 | 0.60 | 0.72 | 2.3629 |
| 31 | 24 | 21 | 14 | 85.60 | 0.9363 | 1.83 | 2.08 | 5.0983 |
| 32 | 24 | 30 | 11 | 25.81 | 0.9770 | 1.48 | 2.68 | 7.1429 |
| 33 | 23 | 30 | 18 | 51.56 | 0.9779 | 2.31 | 2.25 | 6.0099 |
| 34 | 23 | 33 | 18 | 77.61 | 0.9746 | 2.84 | 3.22 | 15.6619 |
| 35 | 23 | 19 | 3 | 112.85 | 0.9244 | 0.37 | 0.25 | 0.5472 |
| 36 | 6 | 12 | 18 | 231.84 | 0.9552 | 0.82 | 1.70 | 5.7461 |
| 37 | 24 | 30 | 14 | 25.69 | 0.9759 | 1.94 | 2.64 | 7.1671 |
| 38 | 23 | 3 | 4 | 100.50 | 0.9301 | 0.43 | 0.25 | 0.4170 |
| 39 | 19 | 2 | 3 | 130.38 | 0.9224 | 0.41 | 0.27 | 0.2267 |
| 40 | 5 | 6 | 26 | 67.69 | 0.9532 | 0.43 | 0.21 | 0.2278 |
| 41 | 29 | 30 | 31 | 193.0 | 0.8980 | 0.33 | 0.34 | 0.6214 |
| 42 | 24 | 23 | 3 | 119.09 | 0.9236 | 0.37 | 0.31 | 0.5472 |
| 43 | 21 | 20 | 19 | 246.34 | 0.9051 | 0.42 | 0.45 | 0.6297 |
| 44 | 4 | 6 | 8 | 52.80 | 0.9630 | 0.44 | 0.64 | 1.5007 |
| 45 | 28 | 30 | 32 | 175.37 | 0.9153 | 0.35 | 0.61 | 1.6249 |
| 46 | 10 | 11 | 12 | 295.94 | 0.8632 | 0.50 | 0.22 | 0.2071 |

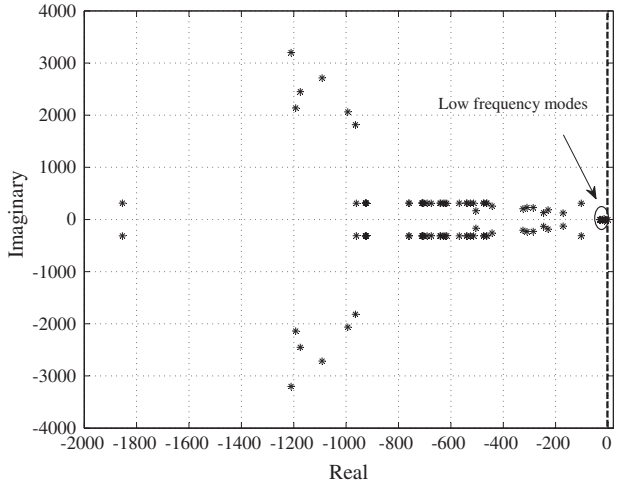


**Fig. 10.** Eigenvalue plot of the microgrid.

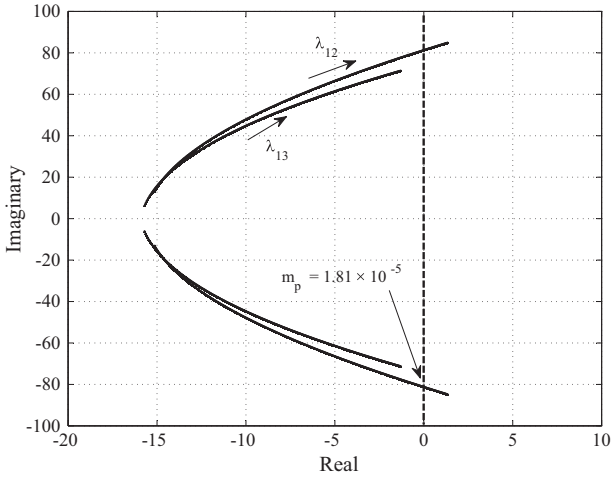


**Fig. 11.** System-3: case-1: Rootlocus plot with variation in droop gain $m_p$.

for placement of generators in this location in [40] was done with separate conditions (grid-connected, exporting power, etc.). From network loss, stability, and voltage perspectives, case −37, case −3 and case −33 are preferred options.

### 3.3.1. Rootlocus analysis

Fig. 10 shows the eigenvalues plot for case −1 (base case). Out of 165 eigenvalues 92 eigenvalues are shown in figure (rest of the eigenvalues are highly damped). For dynamic stability, low-frequency mode Eigenvalues, which are sensitive to the droop gains of the system, are of interest. These low-frequency modes correspond to the power controller mode of the VSI [33,36]. Case −1 (base case), case −3 (highest stability margin), and case −41 (least stability margin) are considered for detailed analysis. Two complex conjugate low-frequency mode trajectories sensitive to real power droop gain for these cases are shown in Figs. 11–13, respectively. $\lambda_{12}$ shows the interaction of low frequency modes between VSIs 1 and 2 while $\lambda_{13}$ shows the interaction of low frequency modes between VSIs 1 and 3. This trajectory shows that $\lambda_{12}$ goes into an unstable mode at a lower value of $m_p$ than $\lambda_{13}$.

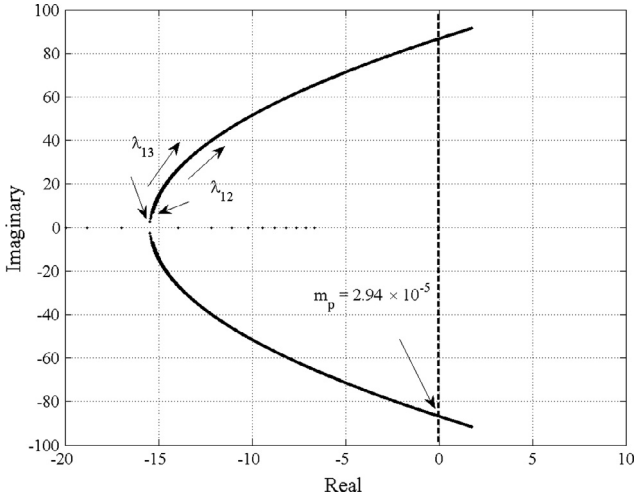


**Fig. 12.** System-3: case-3: Rootlocus plot with variation in droop gain $m_p$.

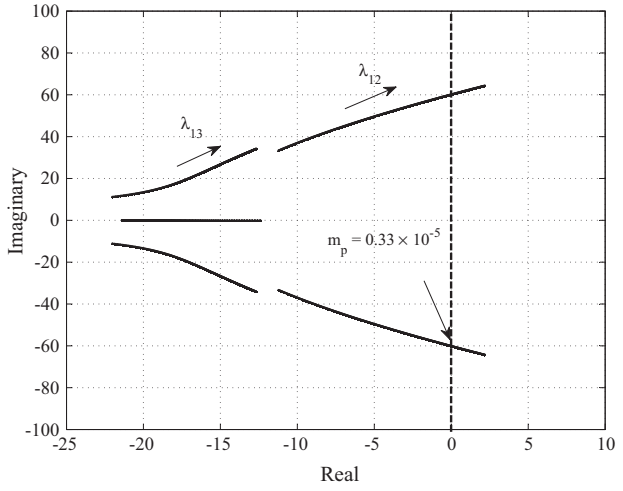


**Fig. 13.** System-3: case-41: Rootlocus plot with variation in droop gain $m_p$.

In Fig. 11, $\lambda_{12}$ starts at $-15.7 \pm$ j 6.2054 and reaches the imaginary axis at $0 \pm$ j 81.265. In Figs. 12 and 13, $\lambda_{12}$ starts from $-15.24 \pm$ j 8.065 and $-11.213 \pm$ j 33.373 and reaches to imaginary axis at $0 \pm$ j 86.75 and $0 \pm$ j 60.118 respectively. From these root locus plots, the impact of minimum distance between sources on stability margin is clearly observed, and it is understood that sources separated with higher impedance have relatively higher stability margin.

To investigate the effect of generator size on power loss and stability margin three more case studies for different size of generators are performed. Locations of DGs are fixed (Case-4, Table 3): DG-1 at node 24, DG-2 at node 30 and DG-3 at node-8. In case-4 size of DGs are in proportion of 1.0:1.0:0.67 p.u. Rest three case studies are performed for the size in proportion of 1:0.728:0.584, 1.0:1.0:1.0 and 1.0:0.561:0.661 p.u. respectively and results are shown in Table 4. From the case studies it is clear that placement of DG is important and by changing the rating of DGs stability margin along with power loss changes. However for this case study minor change in stability margin along with power loss is observed.

### 3.3.2. Pareto front identification

The locations of generators should depend on network losses and overall stability of the system. For multi-objective optimization of the DG network, Pareto optimal front should be identified. Pareto optimal front is defined as a set of non-dominated solutions [41–43]. Data in Table 3 is plotted and Pareto fronts (set of non dominated solutions) obtained between $m_{p,max}$ vs. real power loss and $n_{q,max}$ vs. reactive power loss (Figs. 14 and 15 respectively).

Critical observations from Pareto fronts (for 33-bus system) are:

- Cases corresponding to Pareto fronts (shown in open box) obtained in Fig. 14 are 2, 3, 5 and 37.
- Cases corresponding to Pareto fronts (shown in open box) obtained in Fig. 15 are 2, 3 and 32.
- Case-1 which represents optimal location of sources in a grid-connected system, does not lie on the Pareto front. This clearly indicates that the optimal placement of sources in a grid-connected microgrid is not optimal during islanding.

### 3.4. System 4: 22-bus APEPDCL distribution network

The optimal locations of three generators (in a grid-connected system) based on loss minimization, proposed in [35], are at nodes 12, 14, and 20. System simulation (time domain) is performed with these three generators at various locations (cases) in the 22-bus APEPDCL distribution network. From the operating points, state space matrix is obtained using (3). Root locus analysis is performed for these cases by varying droop constants to identify the stability limit. The values of $m_{p,max}$ and $n_{q,max}$ are noted when the system reaches an unstable region. Losses in the system, minimum voltage

**Table 4**
Case study results for three DGs placement for IEEE 33-bus radial network.

| DG-1 node | DG-2 node | DG-3 node | Size of DGs (p.u.) | $P_{loss}$ (kW) | $V_{min}$ (p.u.) | $m_{p,max}$ ($10^{-5}$) | $n_{q,max}$ ($10^{-4}$) | $Z_{min}$ (Ω) |
|---|---|---|---|---|---|---|---|---|
| 24 | 30 | 8 | 1.0:1.0:0.67 | 32.36 | 0.9694 | 0.92 | 1.80 | 6.1455 |
| 24 | 30 | 8 | 1.0:0.728:0.584 | 26.27 | 0.9690 | 0.90 | 1.78 | 6.1455 |
| 24 | 30 | 8 | 1.0:1.0:1.0 | 26.63 | 0.9687 | 0.85 | 1.75 | 6.1455 |
| 24 | 30 | 8 | 1.0:0.561:0.661 | 25.43 | 0.9688 | 0.89 | 2.01 | 6.1455 |

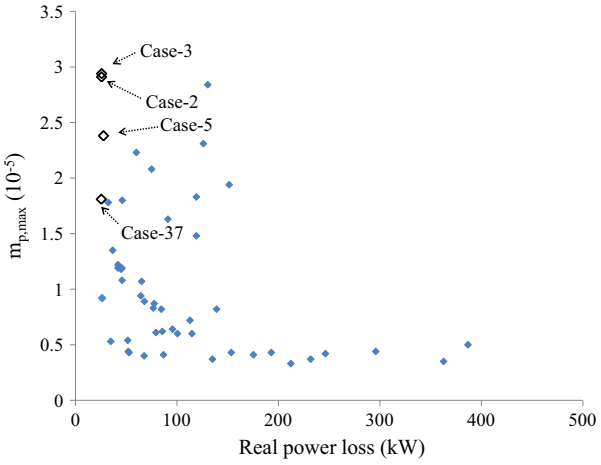


**Fig. 14.** Real power loss vs. $m_{p,max}$ for IEEE 33 bus system with three DGs - Pareto front shown in open boxes.

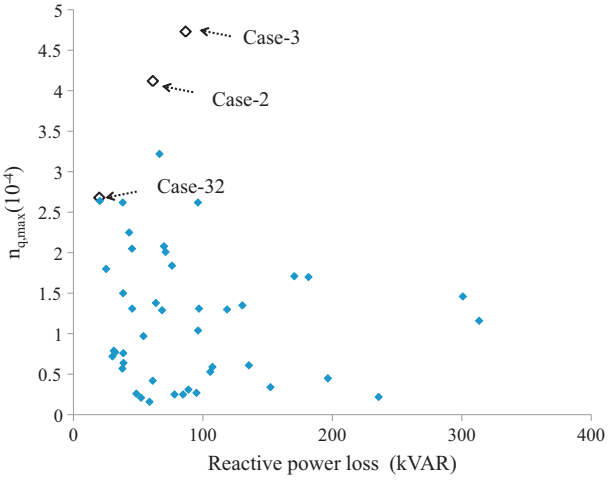


**Fig. 15.** Reactive power loss vs. $n_{q,max}$ for IEEE 33 bus system with three DGs - Pareto front shown in open boxes.

value in the total network, $m_{p,max}, n_{q,max}$, and minimum distance between the DGs for all these cases are presented in Table 5.

It is clear that the maximum values of $m_{p,max}, n_{q,max}$ are not the highest for case 1. This is true since the decision for placement of generators in this location was made with separate conditions (grid-connected, exporting power, etc.). From network loss, stability, and voltage perspectives, case 8, case 6, and case 8 are preferred options. Case 1 (base case), case 6 (highest stability margin) and case 20 (least stability margin) are considered for detailed analysis.

Plots of $m_{p,max}$ vs. $Z_{min}$ (minimum impedance among sources) and $n_{q,max}$ vs. $Z_{min}$ are shown in Figs. 16 and 17, respectively.

### 3.4.1. Rootlocus analysis

Figs. 18–20 show root locus plot for cases 6, 8 and 20, respectively. $\lambda_{12}$ shows the interaction of low-frequency modes between VSIs 1 and 2 while $\lambda_{13}$ shows the interaction of low frequency modes between VSIs 1 and 3. This trajectory shows that $\lambda_{12}$ goes into an unstable mode at a lower value of $m_p$ than $\lambda_{13}$. In Fig. 18 $\lambda_{12}$ starts from an approximate value of $-15.55 \pm j\ 21.27$ and reaches the imaginary axis at an approximate value of $0 \pm j\ 63.3$. In Figs. 19 and 20, $\lambda_{12}$ approximately starts from $-15.27 \pm j\ 15.275$ and $-16.19 \pm j\ 24.70$ and reaches the imaginary axis approximately at $0 \pm j\ 71.1$ and $0 \pm j\ 59.7$ respectively. The following are some critical observations from the case studies:

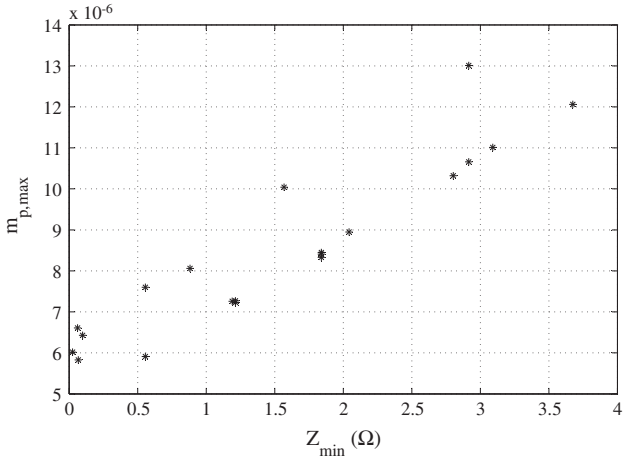


**Fig. 16.** Plot between $m_{p,max}$ vs. $Z_{min}$.

**Table 5**
Various case study results for three DGs placement for APEPDCL 22-bus practical radial network.

| Case | DG-1 node | DG-2 node | DG-3 node | $P_{loss}$ (kW) | $V_{min}$ (p.u.) | $m_{p,max}$ ($10^{-6}$) | $n_{q,max}$ ($10^{-5}$) | $Z_{min}$ (Ω) |
|---|---|---|---|---|---|---|---|---|
| 1 | 12 | 14 | 20 | 0.740 | 0.9952 | 7.23 | 4.48 | 1.2137 |
| 2 | 3 | 14 | 20 | 0.752 | 0.9967 | 7.29 | 4.90 | 1.2137 |
| 3 | 8 | 12 | 22 | 3.154 | 0.9951 | 12.06 | 8.49 | 3.6752 |
| 4 | 8 | 13 | 22 | 2.627 | 0.9958 | 11.01 | 8.04 | 3.0911 |
| 5 | 4 | 15 | 22 | 0.612 | 0.9971 | 8.41 | 6.10 | 1.8402 |
| 6 | 8 | 10 | 22 | 4.4459 | 0.9942 | 13.01 | 8.16 | 2.9157 |
| 7 | 3 | 15 | 22 | 0.953 | 0.9965 | 8.45 | 6.25 | 1.8402 |
| 8 | 4 | 14 | 20 | 0.367 | 0.9972 | 7.26 | 4.85 | 1.1897 |
| 9 | 9 | 15 | 22 | 0.732 | 0.9968 | 8.33 | 5.76 | 1.8402 |
| 10 | 8 | 9 | 17 | 5.078 | 0.9965 | 10.32 | 7.10 | 2.8026 |
| 11 | 3 | 10 | 17 | 3.675 | 0.9965 | 10.04 | 5.60 | 1.5681 |
| 12 | 8 | 11 | 17 | 3.586 | 0.9967 | 8.95 | 6.49 | 2.0428 |
| 13 | 8 | 10 | 18 | 5.041 | 0.9961 | 10.66 | 7.47 | 2.9157 |
| 14 | 12 | 15 | 18 | 0.943 | 0.9953 | 5.91 | 3.49 | 0.5567 |
| 15 | 15 | 18 | 22 | 2.712 | 0.9903 | 7.60 | 3.50 | 0.5567 |
| 16 | 10 | 12 | 15 | 2.050 | 0.9954 | 8.06 | 4.11 | 0.8826 |
| 17 | 13 | 14 | 15 | 1.514 | 0.9945 | 6.02 | 2.13 | 0.0249 |
| 18 | 20 | 21 | 22 | 6.410 | 0.9840 | 6.43 | 2.17 | 0.0980 |
| 19 | 9 | 10 | 11 | 5.281 | 0.9879 | 6.61 | 2.16 | 0.0615 |
| 20 | 6 | 7 | 8 | 19.336 | 0.9683 | 5.83 | 2.15 | 0.0673 |

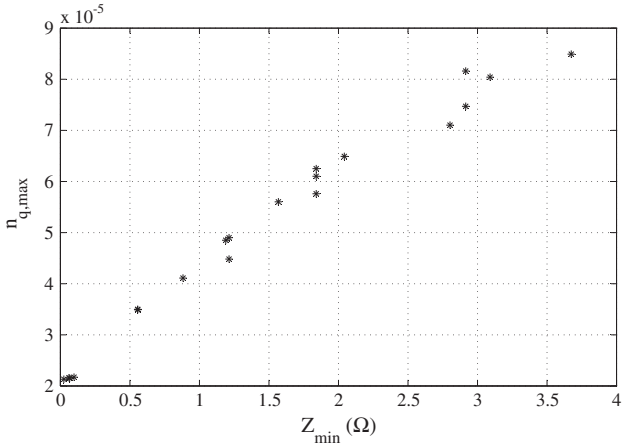


**Fig. 17.** Plot between $n_{q,max}$ vs. $Z_{min}$.

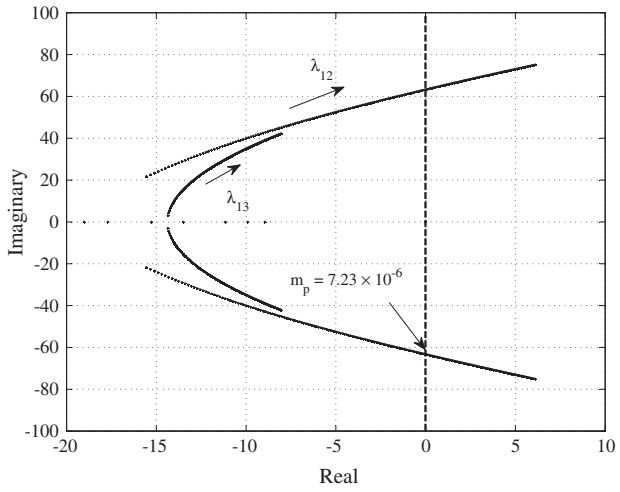


**Fig. 18.** Table 5, case-1: Rootlocus plot with variation in droop gain $m_p$.

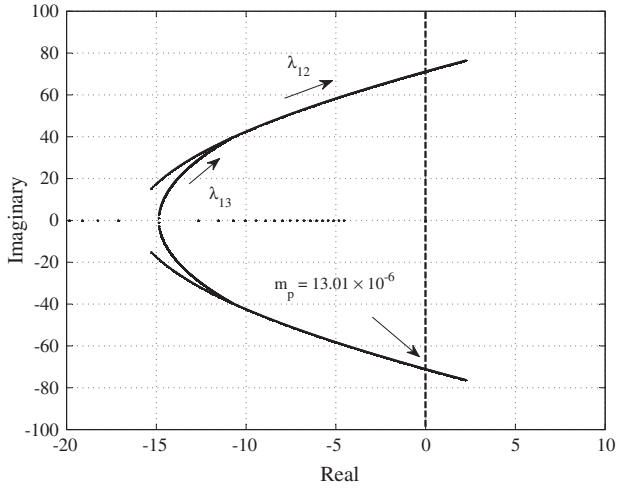


**Fig. 19.** Table 5, case-6: Rootlocus plot with variation in droop gain $m_p$.

- The system configuration (generator location) with low losses in grid connected mode may suffer from stability issues when islanded. This can be a serious problem when the reliability of the main grid is poor.
- The interaction of low-frequency modes between various DGs is different and the location of some inverters is critical (inverter 2 in this case) with respect to the stability.

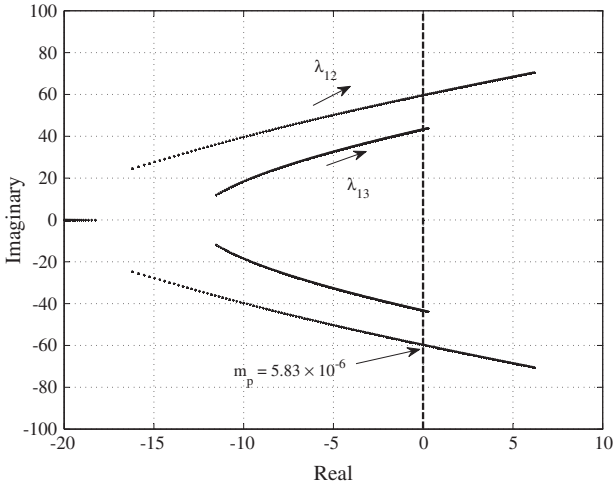


**Fig. 20.** Table 5, case-20: Rootlocus plot with variation in droop gain $m_p$.

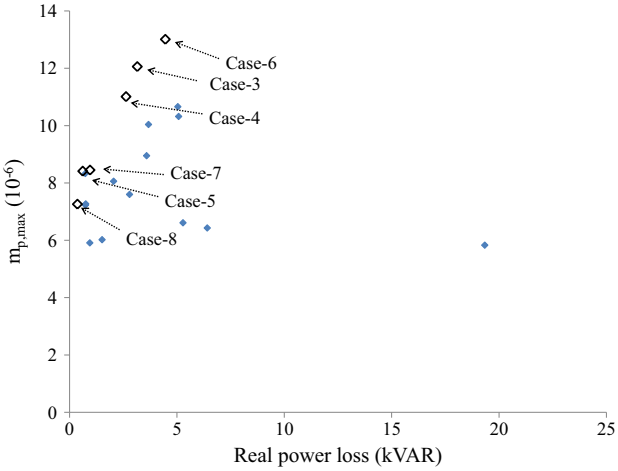


**Fig. 21.** Real power loss vs. $m_{p,max}$ for 22 bus APEPDCL network with three DGs - Pareto front shown in open boxes.

- Stability margin (gain of droop constant) is a function of minimum distance between the generators in an islanded network.
- It is important to choose an optimal location for these generators by considering stability and network losses.

### 3.4.2. Pareto front identification

Pareto optimal front is defined as a set of non-dominated solutions [41–43]. Data in Table 5 is plotted and Pareto front (set of non dominated solutions) obtained between $m_{p,max}$ vs. real power loss and $n_{q,max}$ vs. reactive power loss (Figs. 21 and 22 respectively).

Critical observations from Pareto fronts (for 22 bus practical system) are:

- Cases corresponding to Pareto fronts (shown in open box) obtained in Fig. 21 are 3, 4, 5, 6, 7 and 8.
- Cases corresponding to Pareto fronts (shown in open box) obtained in Fig. 22 are 3, 4, 5, 7 and 8.
- Similar to the previous example, case −1 does not lie on the Pareto front.
- Cases 3,4 and 6 have high stability margin and higher losses, while cases 5, 7, and 8 have low stability margin and low losses.

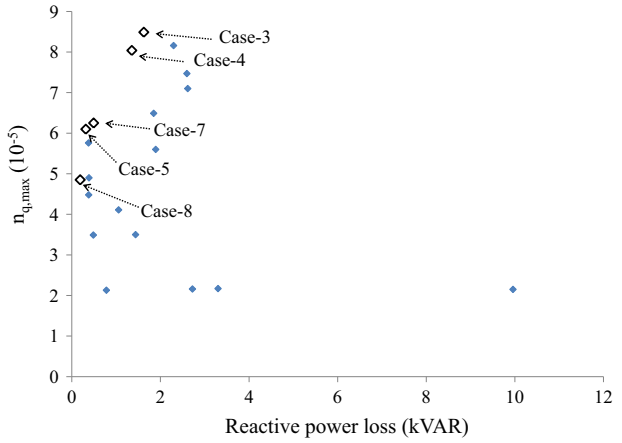


**Fig. 22.** Reactive power loss vs. $n_{q,max}$ for 22 bus APEPDCL network with three DGs - Pareto front shown in open boxes.

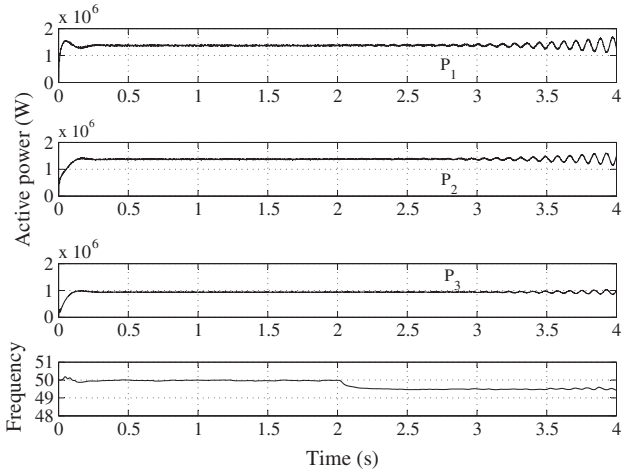


**Fig. 23.** Real power output of DGs and system frequency in Std. IEEE 33 network.

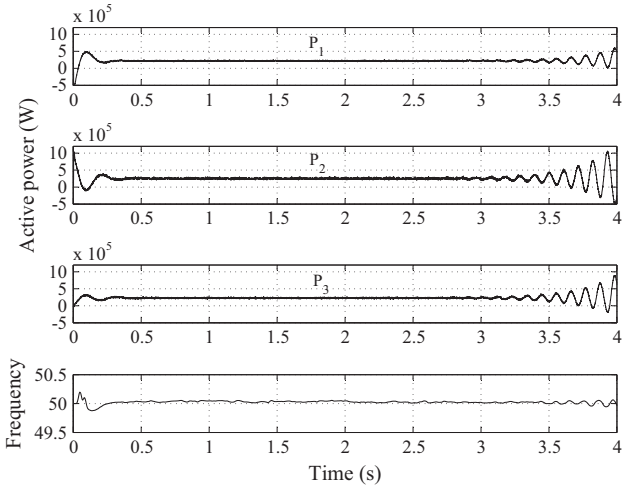


**Fig. 24.** Real power output of DGs and system frequency in practical 22 bus distribution network.

## 4. Simulation – time domain validation

Time domain simulation is performed on both the networks for validation of stability analysis. Simulation results for the three DG system (case −1 of Table 3) and for the practical network (case −1 of Table 5) are shown in Figs. 23 and 24, respectively.

The system is stable and sharing power as per the droop law. The effect of higher value of droop parameter is investigated by changing the droop value (beyond $m_{p,max}$). At time t = 2s for a higher value of $m_p$ ($> m_{p,max}$), power output of DGs is oscillating with increasing amplitude as shown in Fig. 23, which indicates that the system is now unstable.

## 5. Conclusion

The effect of location of droop-based sources on small signal stability, transient response, and network losses in an islanded network is investigated. A modified IEEE 13-bus, IEEE 33-bus system and a 22-bus practical distribution network are chosen for study. A microgrid model is developed for both the networks with droop-based sources, network components, and loads for stability analysis. Higher droop in DGs is desired for better power sharing and transient response. Small signal stability is studied for various locations of DGs (two/three) by varying the droop constant. From the stability study, it is found that a system optimized for losses in grid-connected mode may suffer from small signal stability issues and poor transient response when in islanded configuration. It is also found that the minimum distance between generators in the network has an impact on small signal stability. For multiobjective optimization Reference point based Non-dominated Sorting Genetic Algorithm (R-NSGA) is implemented keeping small signal stability margin and power loss minimization as objectives and Pareto front is obtained. Results of small signal stability analysis are verified using time domain simulation in MATLAB for both the networks.

## References

[1] Thomson M, Infield DG. Impact of widespread photovoltaics generation on distribution systems. IET Renew Power Gener 2007;1(1):33–40.
[2] Soultanis NL, Papathanasiou SA, Hatziargyriou ND. A stability algorithm for the dynamic analysis of inverter dominated unbalanced LV microgrids. IEEE Trans Power Syst 2007;20(1):294–304.
[3] Georgilakis PS, Hatziargyriou ND. Optimal distributed generation placement in power distribution networks: models, methods, and future research. IEEE Trans Power Syst 2013;28(3):3420–8.
[4] Willis HL. Analytical methods and rules of thumb for modeling DG distribution interaction. In: Proc IEEE power eng soc summer meeting. p. 1643–4.
[5] Acharya N, Mahat P, Mithulananthan N. An analytical approach for DG allocation in primary distribution network. Int J Electr Power Energy Syst 2006;28(10):669–78.
[6] Hung DQ, Mithulananthan N. Loss reduction and loadability enhancement with DG: a dual-index analytical approach. Appl Energy 2014;115:233–41.
[7] Fua X, Chena H, Caic R, Yang P. Optimal allocation and adaptive VAR control of PV-DG in distribution networks. Appl Energy 2015;137(1):173–82.
[8] Hung DQ, Mithulananthan N, Bansal RC. Analytical strategies for renewable distributed generation integration considering energy loss minimization. Appl Energy 2013;105:75–85.
[9] Sheng W, Liu K, Meng X, Ye X, Liu Yongmei. Research and practice on typical modes and optimal allocation method for PV-wind-ES in microgrid. Electr Power Syst Res 2015;120(10):242–55.
[10] Sfikas EE, Katsigiannis YA, Georgilakis PS. Simultaneous capacity optimization of distributed generation and storage in medium voltage microgrids. Electr Power Syst Res 2015;67:101–13.
[11] Moradia MH, Eskandarib M, Showkatia H. A hybrid method for simultaneous optimization of DG capacity and operational strategy in microgrids utilizing renewable energy resources. Electr Power Energy Syst 2014;56(3):241–58.
[12] Khodaei A. Microgrid optimal scheduling with multi-period islanding constraints. IEEE Trans Power Syst 2014;29(3):1383–92.
[13] Conti S, Nicolosi R, Rizzo SA, Zeineldin HH. Optimal dispatching of distributed generators and storage systems for MV islanded microgrids. IEEE Trans Power Del 2012;27(3):1243–51.

[14] Ahn SJ, Nam SR, Choi JH, Moon S. Power scheduling of distributed generators for economic and stable operation of a microgrid. IEEE Trans Smart Grid 2013;4(1):398–405.
[15] Gomeza M, Lopezb A, Juradoa F. Optimal placement and sizing from standpoint of the investor of photovoltaics grid-connected systems using binary particle swarm optimization. Appl Energy 2010;87(6):1911–8.
[16] Rena H, Zhoub W, Nakagamib K, Gaoc W, Wuc Q. Multi-objective optimization for the operation of distributed energy systems considering economic and environmental aspects. Appl Energy 2010;87(12):3642–51.
[17] Niknama T, Taheria SI, Aghaeia J, Tabatabaeib S, Nayeripoura M. A modified honey bee mating optimization algorithm for multiobjective placement of renewable energy resources. Appl Energy 2011;88(12):4817–30.
[18] Abdelaziz MMA, El-Saadany EF. Maximum loadability consideration in droop-controlled islanded microgrids optimal power flow. Electr Power Syst Res 2014;10(6):168–79.
[19] Abdelaziz MMA, El-Saadany EF, Seethapathy R. Assessment of droop-controlled islanded microgrid maximum loadability. IEEE PES Gen Meet 2013:1–5.
[20] Abdelaziz MMA, El-Saadany EF. Determination of worst case loading margin of droop-controlled islanded microgrids. In: IEEE international conference on electric power and energy conversion systems (EPECS). p. 1–6.
[21] Gampa SR, Das D. Optimum placement and sizing of DGs considering average hourly variations of load. Electr Power Energy Syst 2015;66:25–40.
[22] Soroudi A, Ehsan M. IGDT based robust decision making tool for DNOs in load procurement under severe uncertainty. IEEE Trans Smart Grid 2013;4(2):886–95.
[23] Khadem SK, Basu M, Conlon MF. A comparative analysis of placement and control of UPQC in DG integrated grid connected network. Sustain Energy Grids Netw 2016;6:46–57.
[24] Abdelaziz MMA, El-Saadany EF. Economic droop parameter selection for autonomous microgrids including wind turbines. Renew Energy 2014:393–404.
[25] Yan B, Wang B, Tang F, Liu D, Ma Z, Shao Y. Development of economics and stable power-sharing scheme in autonomous microgrid with volatile wind power generation. Electr Power Compon Syst 2014;42(12):1313–23.
[26] Wu X, Shen C, Zhao M, Wang Z, Huang X. Small signal security region of droop coefficients in autonomous microgrids. IEEE PES Gen Meet 2014:1–5.
[27] Meegahapola LG, Robinson D, Agalgaonkar AP, Perera S, Ciufo P. Microgrids of commercial buildings: strategies to manage mode transfer from grid connected to islanded mode. IEEE Trans Sust Energy 2014;5(4):1337–47.
[28] Barklund E, Pogaku N, Prodanvoic M, Hernandez-Aramburo C, Green TC. Energy management in autonomous microgrid using stability-constrained droop control of inverters. IEEE Trans Power Electron 2008;23(5):2346–52.
[29] Dfaz G, Moran CG, Aleixandre JG, Diez A. Scheduling of droop coefficients for frequency and voltage regulation in isolated microgrids. IEEE Trans Power Syst 2010;25(1):489–96.
[30] Paquette AD, Reno MJ, Harley RG, Diwan DM. Transient load sharing between inverters and synchronous generators in islanded microgrids. In: IEEE energy conversion congress and exposition (ECCE). p. 2735–42.
[31] Hassan MA, Abido MA. Optimal design of microgrids in autonomous and grid-connected modes using particle swarm optimization. IEEE Trans Power Electron 2011;26(3):755–69.
[32] Chung IY, Liu W, Cartes DA, Collins EG, Moon SI. Control methods of inverter-interfaced distributed generators in a microgrid system. IEEE Trans Ind Appl 2010;46(3):1078–88.
[33] Dheer DK, Soni N, Doolla S. Improvement of small signal stability margin and transient response in inverter-dominated microgrids. Sustain Energy Grids Netw 2016;5:135–47.
[34] Venkatesh B, Ranjan R, Gooi HB. Optimal reconfiguration of radial distribution systems to maximize loadability. IEEE Trans Power Syst 2004;19(1):260–6.
[35] Raju MR, Murthy KVSR, Ravindra K. Direct search algorithm for capacitive compensation in radial distribution systems. Electr Power Energy Syst 2012;42(1):24–30.
[36] Pogaku N, Prodanovic M, Green TC. Modeling, analysis and testing of autonomous operation of an inverter-based microgrid. IEEE Trans Power Electron 2007;22(2):613–25.
[37] Siegmund F, Bernedixn J, Pehrsson L, Ng AHC, Deb K. Reference point-based evolutionary multi-objective optimization for industrial system simulation. In: Winter simulation conference-2012, Berlin, Germany.
[38] Filatovas E, Lancinskas A, Kurasova O, Zilinskas J. A preference-based multi-objective evolutionary algorithm R-NSGA-II with stochastic local search. Central Eur J Oper Res 2016:1–20. http://dx.doi.org/10.1007/s10100-016-0443-x.
[39] Lazoglou M, Kolokoussis P, Dimopoulou E. Investigating the use of a modified NSGA-II solution for land-use planning in mediterranean islands. J Geogr Inform Syst 2016;8:369–86.
[40] Hung DQ, Mithulananthan N. Multiple distributed generator placement in primary distribution networks for loss reduction. IEEE Trans Ind Electr 2013;60(4):1700–8.
[41] Sahoo NC, Ganguly S, Das D. Fuzzy-Pareto-dominance driven possibilistic model based planning of electrical distribution systems using multi-objective particle swarm optimization. Expert Syst Appl 2012;39:881–93.
[42] Ganguly S, Sahoo NC, Das D. Multi-objective planning of electrical distribution systems using dynamic programming. Electr Power Energy Syst 2013;46:65–78.
[43] Deb K, Pratap A, Agarwal S, Meyarivan T. A fast and elitist multiobjective genetic algorithm: NSGA-II. IEEE Trans Evol Comput 2002;6:182–97.